Journal of Molecular Graphics and Modelling 29 (2011) 1039–1046

Contents lists available at ScienceDirect

Journal of Molecular Graphics and Modelling

journal homepage: www.elsevier.com/locate/JMGM

Probing the reactivation process of sarin-inhibited acetylcholinesterase with α-nucleophiles: Hydroxylamine anion is predicted to be a better antidote with DFT calculations

Md Abdul Shafeeuulla Khan[a], Rabindranath Lo[a], Tusar Bandyopadhyay[b], Bishwajit Ganguly[a,*]

[a] Analytical Science Discipline, Central Salt & Marine Chemicals Research Institute (Council of Scientific and Industrial Research), Bhavnagar, Gujarat 364 002, India
[b] Theoretical Chemistry Section, Chemistry Group, Bhabha Atomic Research Centre, Trombay, Mumbai 400 085, India

ARTICLE INFO

Article history:
Received 8 February 2011
Received in revised form 22 April 2011
Accepted 27 April 2011
Available online 6 May 2011

Keywords:
Reactivation
OP-inihited AChE
Alpha-nucleophiles
Density functional calculations
Hydroxylamine anion

ABSTRACT

Inactivation of acetylcholinesterase (AChE) due to inhibition by organophosphorus (OP) compounds is a major threat to human since AChE is a key enzyme in neurotransmission process. Oximes are used as potential reactivators of OP-inhibited AChE due to their α-effect nucleophilic reactivity. In search of more effective reactivating agents, model studies have shown that α-effect is not so important for dephosphylation reactions. We report the importance of α-effect of nucleophilic reactivity towards the reactivation of OP-inhibited AChE with hydroxylamine anion. We have demonstrated with DFT [B3LYP/6-311G(d,p)] calculations that the reactivation process of sarin–serine adduct 2 with hydroxylamine anion is more efficient than the other nucleophiles reported. The superiority of hydroxylamine anion to reactivate the sarin-inhibited AChE with sarin–serine adducts 3 and 4 compared to formoximate anion was observed in the presence and absence of hydrogen bonding interactions of Gly121 and Gly122. The calculated results show that the rates of reactivation process of adduct 4 with hydroxylamine anion are 261 and 223 times faster than the formoximate anion in the absence and presence of such hydrogen bonding interactions. The DFT calculated results shed light on the importance of the adjacent carbonyl group of Glu202 for the reactivation of sarin–serine adduct, in particular with formoximate anion. The reverse reactivation reaction between hydroxylamine anion and sarin–serine adduct was found to be higher in energy compared to the other nucleophiles, which suggests that this α-nucleophile can be a good antidote agent for the reactivation process.

1. Introduction

Many persistent chemicals such as paraoxon, parathion and chemical warfare compounds such as VX, sarin, etc. are hydrophobic phosphorus (V) esters or phosphylating agents. They can irreversibly react with the enzyme acetylcholinesterase (AChE), inhibiting its control over the central nervous system [1–3]. AChE catalyzes the ester hydrolysis process of the neurotransmitter acetylcholine (ACh) to terminate synaptic transmission [4–6]. Inhibition of AChE occurs as a result of the phosphylation of the active serine residue with organophosphorus compounds [7–9]. Such AChE inhibition results in acetylcholine accumulation at cholinergic receptor sites, thereby excessively stimulating the cholinergic receptors. This can lead to various clinical disorders sometimes causes death. Therefore, reactivation of organophosphorus compound inhibited AChE is necessary to get back its catalytic activity towards the hydrolysis of ACh. The inhibited AChE may further undergo "aging" process that normally involves dealkylation or deamidation depending upon the nature of organophosphorus compounds attacked and is irreversible in nature [10–12]. Therefore, there is a need to develop efficient reactivators for the OP-inhibited AChE. Computational methods offer an ability to explore these types of reactions [3,12–24] while avoiding exposure to these deadly agents. Hence, it is quite useful in suggesting new nucleophiles with greater efficiency for the reactivation of inhibited AChE. It has been reported that α-nucleophiles such as oximes are able to reactivate organophosphate–cholinesterase conjugates, giving rise to free enzyme [22]. In our previous studies, we have reported that hydroxylamine anion (NH_2O^-) is an efficient α-nucleophile for the detoxification of the organophosphorus compounds such as VX and sarin [20]. In this article, we report the efficacy of NH_2O^- towards the reactivation of sarin-inhibited AChE adduct.

2. Computational methodology

The following protocol was used to generate conformations of modeled sarin–serine adduct. (i) An exhaustive conformational

* Corresponding author. Fax: +91 278 2567562.
E-mail address: ganguly@csmcri.org (B. Ganguly).

1093-3263/$ – see front matter © 2011 Elsevier Inc. All rights reserved.
doi:10.1016/j.jmgm.2011.04.009

search was performed with the molecular modeling program Macromodel [25] using MMFFs force field [26–30]. Energy minimizations were performed with the Polak–Ribiere conjugate gradient (PRCG) method [31], which involves the use of first derivatives with convergence criterion set to 0.05 kJ/Å-mol. Conformational search was performed with the random variation of all of the rotatable bonds and combining the Monte Carlo conformational search (MCMM) algorithm [32,33] using 5000 Monte Carlo steps. (ii) Sort all found conformations according to energy. (iii) Stored conformations whose relative energy was within 50 kJ/mol of the lowest energy structure. The resulting conformations were clustered based on torsional RMS using XCluster approach [34]. Based on the minimum separation ratio, we have selected clustering level with two clusters. Minimum separation ratio was employed to find the clustering level at which the distance between members of the clusters is much smaller than the distance between the clusters [35]. Two representative adducts were selected from this clusterization process. The selected conformations from the conformational families were stored for further higher level DFT calculations.

All geometries were optimized using the B3LYP [36–38] density functional and the 6-311G(d,p) basis set. Harmonic frequency calculations at the same level were used to confirm the stationary points and to calculate thermodynamic corrections. Single-point calculations were performed at the B3LYP/6-311 + G(d,p) level to get accurate energies using B3LYP/6-311G(d,p) geometries. Aqueous free energies of solvation of the gas-phase structures were determined with the polarizable continuum model (PCM) [39–43]. Intrinsic reaction coordinate (IRC) calculations were performed to connect all the transition states with their corresponding minima [44,45]. All quantum chemical calculations were performed using Gaussian 03, Revision E.01 program [46].

3. Results and discussion

Solvolysis of sarin and VX with hydroxylamine anion was found to be a very efficient process towards the detoxification of such organophosphorus compounds [20,21]. Generally, it follows the addition–elimination pathway involving a trigonal bipyramidal intermediate. Recent studies have shown that the reactivation process of sarin-inhibited AChE adduct with nucleophiles also involves addition–elimination pathways [22,24]. The reaction energy profile generated for hydroxylamine anion with the sarin-inhibited AChE adduct also follows the addition–elimination pathway involving a trigonal bipyramidal intermediate. The formation of sarin–serine adduct is generally take place by two-step addition–elimination mechanism where serine moiety replaces fluoride ion (Scheme S1 of the supplementary data) [8]. Initially, we have performed an extensive conformational search on sarin–serine adduct as a model for sarin-inhibited AChE due to its flexibility. Two unique conformers of sarin–serine adduct were identified in the conformational search process using MMFFs force field in aqueous phase (GB/SA) after clusterization of the conformations. The computed energy difference between these two adducts is 0.8 kcal/mol. These adducts were further optimized at B3LYP/6-311G(d,p) level of theory, which leads to a larger energy difference of 2.4 kcal/mol (Fig. 1). The conformational difference between these two adducts is due to the orientation of –NHCHO group of serine moiety. In adduct 1, there is a strong intramolecular hydrogen bond between the hydrogen of the –NH group and the oxygen atom of the phosphoryl group (Fig. 1), which leads to a greater stabilization than the adduct 2. The crystal structure of sarin inhibited AChE reported in the literature shows that the intramolecular hydrogen bonding is not present between sarin and serine moiety [47]. Therefore, both adducts 1 and 2 have been considered to examine the efficacy of hydroxylamine anion for the reactivation process.

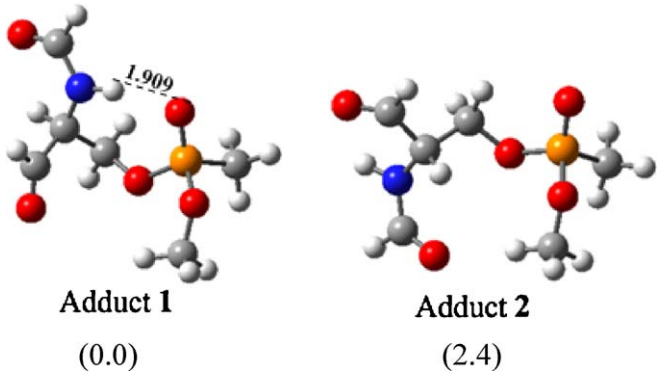

Fig. 1. B3LYP/6-311G(d,p) optimized geometries of two unique conformers of sarin–serine adduct and their relative energies (kcal/mol) (grey = carbon, red = oxygen, blue = nitrogen, white = hydrogen and orange = phosphorus). (For interpretation of the references to color in this figure legend, the reader is referred to the web version of the article.)

The Gibbs free energy with B3LYP/6-311G(d,p) for the reaction between sarin–serine adduct 1 and hydroxylamine anion has been shown in Fig. 2a and the corresponding geometries of stationary points in Fig. 3a. For sarin–serine adduct, the isopropyl group of the sarin moiety was modeled by a methyl group as reported in previous studies [22,24]. Two complexes and two intermediates have been located as local minima on the potential energy surface. Three corresponding transition state structures that link these minima have also been located as first-order saddle points. The intrinsic reaction coordinate (IRC) calculations connect the transition states to the respective minima. The sarin–serine adduct 1 and the hydroxylamine anion forms a complex (C1a), which is energetically stable by 37.6 kcal/mol than the separated reactants. The anionic nucleophile and sarin adduct stabilizes through charge dipole type interactions besides two C–H···O type hydrogen bonds in the complex C1a (Fig. 3a). The free energy of activation computed for the attack of NH_2O^- to the sarin phosphorus atom is 3.2 kcal/mol compared to the complex C1a. NH_2O^- approaches opposite to the oxygen atom of serine moiety in a slightly nonlinear fashion ($\angle$O–P–O = 165.4°) and the P···ONH_2 bond distance is 3.020 Å (TS1a) (Fig. 3a). The Wiberg bond index calculated for the P···ONH_2 distance of TS1a has been found to be 0.05 au, which is about 0.03 au higher than that of C1a signifying a stronger interaction in the former case. In this transition state, N–H···O hydrogen bonding (2.528 Å) has been observed between the nucleophile and the P=O bond of sarin–serine adduct 1 (Fig. 3a) besides the C–H···O type interactions. After TS1a, TBP intermediate IN1a has been found to be 14.5 kcal/mol stable than complex C1a. The –P–ONH_2 bond distance and the bond distance between P and oxygen atom of serine are 1.798 Å and 1.815 Å, respectively in IN1a with the corresponding bond indexes of 0.53 and 0.48 reveals the strengthening and weakening of the corresponding bonds compared to TS1a. The hydrogen-bonding interaction between the nucleophile and the P=O bond of sarin–serine adduct 1 becomes stronger with the shortening of H-bond distance (2.008 Å) in IN1a (Fig. 3a).

To stabilize the leaving group, methoxy group rotates towards the serine moiety of sarin–serine adduct through a rotational transition state TS2a of imaginary frequency 86i cm^{-1} and forms another TBP intermediate IN2a (Fig. 2a). The elimination of the leaving serine group is exergonic in nature and requires only 3.7 kcal/mol free energy of activation (TS3a) from the intermediate IN2a. The Wiberg bond index of 0.66 au for P–ONH_2 further suggests the stronger interaction and the smaller bond index of 0.08 au for the distance between P and the oxygen atom of serine indicates the

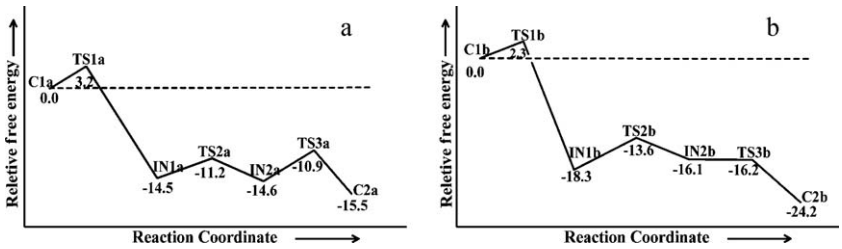

Fig. 2. B3LYP/6-311G(d,p) calculated free energy (kcal/mol) profile diagrams for the reactivation of sarin–serine: (a) adduct 1 and (b) adduct 2 with hydroxylamine anion in gas phase.

expulsion of the leaving group. The forward direction IRC calculation of TS3a leads a complex (C2a) between the sarin moiety and the leaving group at a distance of 3.365 Å. The reactivation process between the hydroxylamine anion and the sarin–serine adduct 1 is governed by the first step and the subsequent steps are downhill in nature at B3LYP/6-311G(d,p) level of theory. The aqueous phase calculations performed at the same level of theory predict the similar potential energy surface as observed in the gas phase calculations (Fig. S1a of the supplementary data).

The Gibbs free energy profile computed at the same level of theory for the reaction between sarin–serine adduct 2 and hydroxylamine anion has been shown in Fig. 2b and the corresponding geometries of stationary points in Fig. 3b. The computed results show that the activation barrier for the interaction of hydroxylamine anion with adduct 2 is lower by 0.9 kcal/mol than the corresponding barrier for 1 (Fig. 2a). The P–ONH_2 bond distance is 3.004 Å (TS1b) (Fig. 3b) and the Wiberg bond order calculated for the P–ONH_2 distance of TS1b has been found to be 0.05 au which is about 0.03 au higher than that of C1b suggests a stronger interaction in the former case. TBP intermediate IN1b has been found to be 18.3 kcal/mol stable than complex C1b. The subsequent stationary points calculated for adduct 2 were found to be similar to that of 1.

The calculated free energy of activation computed at the same level of theory for the reaction of hydroxylamine anion with sarin–serine adduct 2 is 2.3 kcal/mol, which is lower than the free energy of activations of all other nucleophiles reported with the adduct similar to 2 [22,24]. The free energy of activation for the reactivation process of formoximate anion with sarin–serine adduct 2 was found to be 6.4 kcal/mol in the gas phase, whereas, 5.1 kcal/mol was predicted for hydrazonate used as a model reactivation agent of sarin-inhibited AChE. Further, the reactivation process requires only 3.1 kcal/mol of electronic energy with ZPVE correction (Table 1), which is again lower compared to the elec-

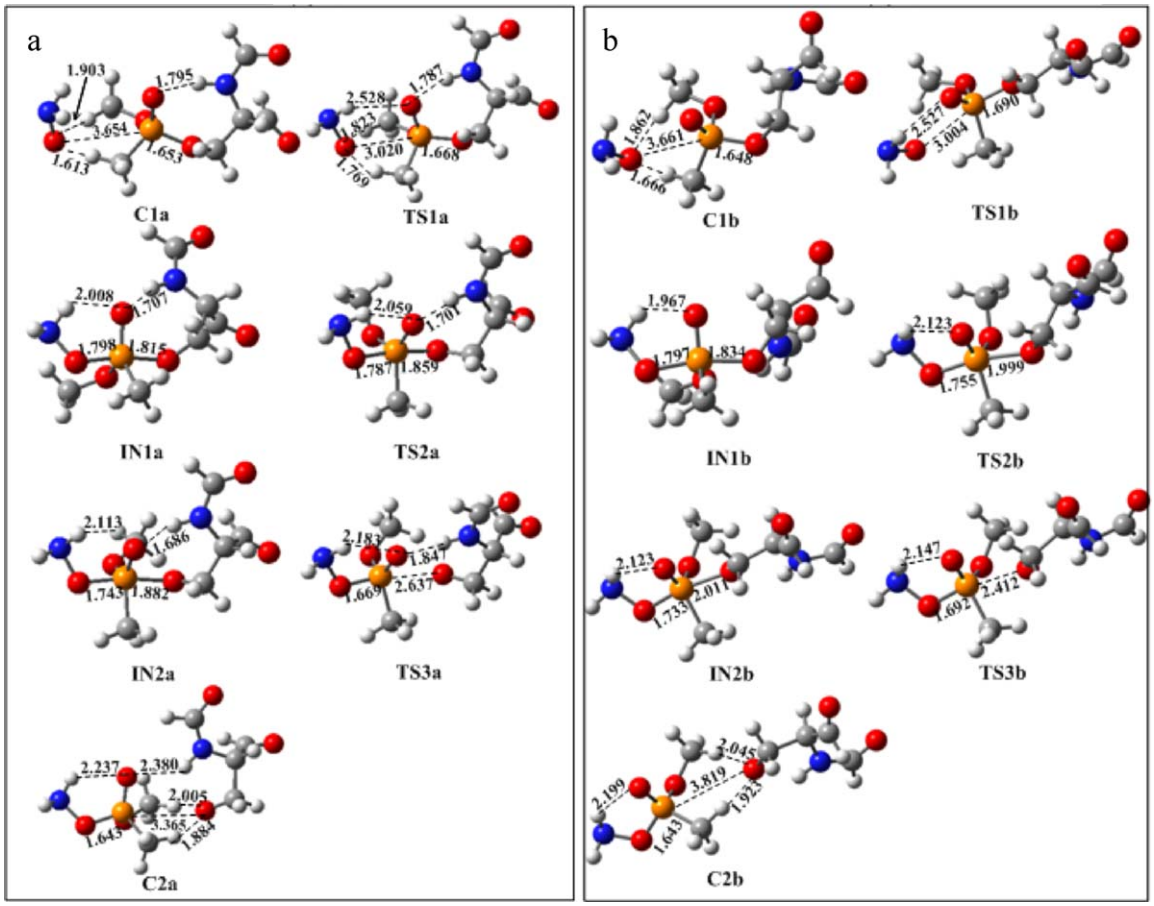

Fig. 3. B3LYP/6-311G(d,p) optimized geometries and selected bond distances (Å) for modeled sarin–serine: (a) adduct 1 and (b) adduct 2 involved in the reactivation process with hydroxylamine anion in gas phase (grey = carbon, red = oxygen; blue = nitrogen; white = hydrogen; orange = phosphorus). (For interpretation of the references to color in this figure legend, the reader is referred to the web version of the article.)

Table 1
The B3LYP/6-311G(d,p) calculated energetic data in gas phase for the reactivation process of adduct 2 given in kcal/mol.

Structure	ΔE	ΔE_{ZPE}	ΔG°
C1	0.0	0.0	0.0
TS1	4.0	3.1	2.3
IN1	−21.6	−19.8	−18.3
TS2	−15.6	−14.8	−13.6
IN2	−17.1	−16.2	−16.1
TS3	−16.3	−16.1	−16.2
C2	−21.9	−22.2	−24.2

tronic energy barriers reported with other nucleophiles [22,24]. We have calculated the rate constants from Gibbs free energies of activation for the rate determining steps of reactions involving hydroxylamine anion and the reported nucleophiles with sarin–serine adduct 2. The first order rate constants for the reactivation reactions involving formoximate, acetaldehyde enolate, methylperoxyle, methylsulphenate, formaldehyde hydrazonate and hydroxylamine anion are $1.3 \times 10^8\ s^{-1}$, $1.7 \times 10^7\ s^{-1}$, $1.9 \times 10^9\ s^{-1}$, $1.3 \times 10^8\ s^{-1}$, $1.1 \times 10^9\ s^{-1}$, $1.3 \times 10^{11}\ s^{-1}$, respectively. The calculated rate constant results further indicate that the NH_2O^- should be faster by 1000 times, 7647 times, 68 times, 1000 times and 118 times than formoximate anion, acetaldehyde enolate, methylperoxyle, methylsulphenate and formaldehyde hydrazonate, respectively.

The potential energy profile further suggests that the free energy activation barrier of the rate determining step for the inverse reactivation with NH_2O^- is 26.5 kcal/mol, which is much higher compared to the inverse reactivations reported with other nucleophiles (Table 2) [24].

To examine the effect of solvent on the reactivation of sarin inhibited AChE, single point calculations at B3LYP/6-311G(d,p) have been performed using polarizable continuum model (PCM) in aqueous solution. The electronic energies of the stationary points predicted in the aqueous phase for the reaction of NH_2O^- with sarin–serine adduct 2 is slightly lower than the corresponding gas phase results (Fig. S1b of the supplementary data and Table 1). The solvent phase calculations showed that the TS3b is 2.1 kcal/mol higher in energy than the intermediate IN2b (Fig. S1b of the supplementary data and Fig. 2b). Further, diffuse function was added in the basis set to describe the negative charge and atoms with isolated electron pairs in the calculations. The results obtained at B3LYP/6-311 + G(d,p)//B3LYP/6-311G(d,p) in both gas and aqueous phases suggest that the reactivation process of sarin–serine adduct 2 with hydroxylamine anion is faster than that of the other nucleophiles reported (Table 3) [24].

The calculations performed with sarin–serine adducts 1 and 2 showed that the hydroxylamine anion would interact with the later adduct more favourably than the former one. To note that the sarin–serine adducts were modeled with the methyl group instead of isopropyl group for direct comparison of results reported with other nucleophiles [22,24]. Further, we have extended our study with the isopropyl group in the sarin–serine adduct 3 (Fig. 4) to examine the effect of such substituent on the PES. Additionally, the carbonyl group attached to the –NH nitrogen in the adduct 2 was not considered in this model system 3 because this carbonyl group comes from Glu202 in the AChE and hence it is not a part of serine moiety (Fig. 4).

The adduct 3 has been taken to examine the reactivation process with hydroxylamine anion and formoximate anion. Formoximate anion has been chosen because oximes exhibit various antidote effects on the OP-inhibited AChE. The PES for the reactivation process of adduct 3 with hydroxylamine anion is given in Fig. 5a and the corresponding optimized geometries are given in Fig. 6a. Hydroxylamine anion showed the similar potential energy surface

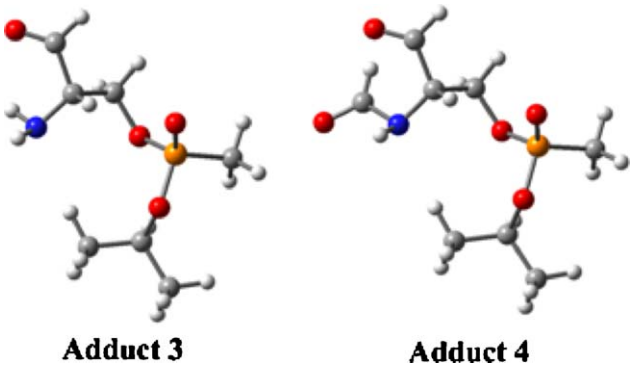

Fig. 4. Sarin–serine adducts 3 and 4 considered for the reactivation process with hydroxylamine and formoximate anions (grey = carbon, red = oxygen, blue = nitrogen, white = hydrogen and orange = phosphorus). (For interpretation of the references to color in this figure legend, the reader is referred to the web version of the article.)

as obtained with the adduct 2. The reaction of hydroxylamine anion with the adduct 3 is a three step process towards the reactivation of sarin inhibited AChE. The rate determining step in this process is initial attack of the nucleophile to the sarin of the sarin–serine adduct 3. The subsequent steps are exergonic in nature. The energies of the stationary points predicted in the aqueous phase for the reaction of NH_2O^- with sarin–serine adduct 3 are similar to that of the gas phase results (Fig. 5a and Fig. S1c of the supplementary data).

Turning to examine the reactivation process of adduct 3 with formoximate anion, the calculations have been performed at the same level of theory. The computed Gibbs free energy profile is given in Fig. 5b and the corresponding optimized geometries are given in Fig. 6b. The reactions of formoximate anion with the adduct 3 is also a three step process towards the reactivation of sarin inhibited AChE as observed in previous cases [22]. However, the rate determining step in the PES is the final step, where the serine moiety is leaving from the sarin of the sarin–serine adduct 3 in contrast to the reported results [22] using the sarin–serine adduct similar to 2 (Fig. 1). The calculated activation barrier for the interaction of formoximate anion with 3 is 11.8 kcal/mol. The overall process is endergonic in nature, which is exergonic with the reported adduct [22]. The aqueous phase calculations showed the similar reaction energy profile as observed in the gas phase results (Fig. 5b and Fig. S1d of the supplementary data).

Examining the geometries obtained from the reactions of adduct 3 with formoximate anion and the corresponding reported geometries [22] with the same anion, it appears that the carbonyl group of Glu202 is playing a role to stabilize the final step of the reactivation process. The leaving serine moiety gets stabilized by the intramolecular hydrogen bonding between the oxyanion and the –NH hydrogen atom of the serine moiety in the reported reaction energy profile of formoximate anion and the sarin–serine adduct [22]. To confirm that, we have performed additional calculations with the adduct 4 having the carbonyl group attached to –NH of the serine moiety (Fig. 4). The PES for the reactivation process of adduct 4 with formoximate anion is given in Fig. 7a and the corresponding optimized geometries are given in Fig. 8a. The calculated results show that the initial attack of the formoximate anion to the adduct 4 is the rate determining step with an activation barrier of 8.7 kcal/mol. The overall process is exergonic in nature (Fig. 7a). The reaction energy profile is now similar to that of the reported profile [22]. Therefore, it is clear that the carbonyl group of adjacent Glu202 is playing an important role to facilitate the reactivation process with formoximate anion. The aqueous phase calculations for adduct 4 showed the similar PES as observed

Table 2
Gibbs free energy activation barriers at B3LYP/6-311G(d,p) in gas phase for the direct and inverse reactivation reactions for 2 in kcal/mol.

Reactivation	NH_2O^- [a]	Oximate[b]	Enolate[b]	Peroxile[b]	Hydrazonate[b]	Sulphenate[b]
Direct	2.3	6.4	7.6	4.8	5.1	6.4
Inverse	26.5	10.7	8.1	16.5	18.6	10.2

[a] Present study.
[b] Data taken from Refs. [22,24].

Table 3
Electronic energy activation barriers at B3LYP/6-311 + G(d,p) in gas and aqueous phases using B3LYP/6-311G(d,p) gas phase optimized geometries.

Reactivation	NH_2O^- [a]	Oximate[b]	Enolate[b]	Peroxile[b]	Hydrazonate[b]	Sulphenate[b]
Gas phase	2.3	6.7	6.8	4.3	3.5	5.1
Aqueous phase	2.3	10.2	13.3	4.2	3.6	8.7

[a] Present study.
[b] Data taken from Ref. [24].

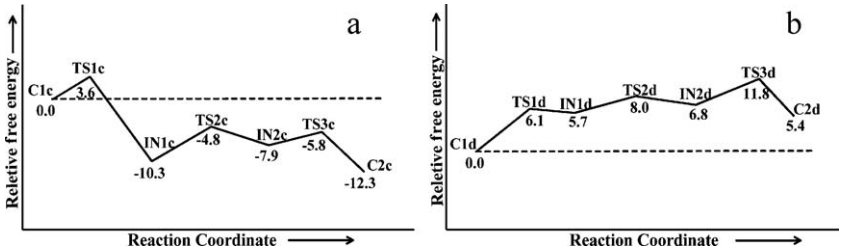

Fig. 5. B3LYP/6-311G(d,p) calculated free energy (kcal/mol) profile diagrams for the reactivation of sarin–serine adduct 3 with: (a) hydroxylamine anion and (b) formoximate anion in gas phase.

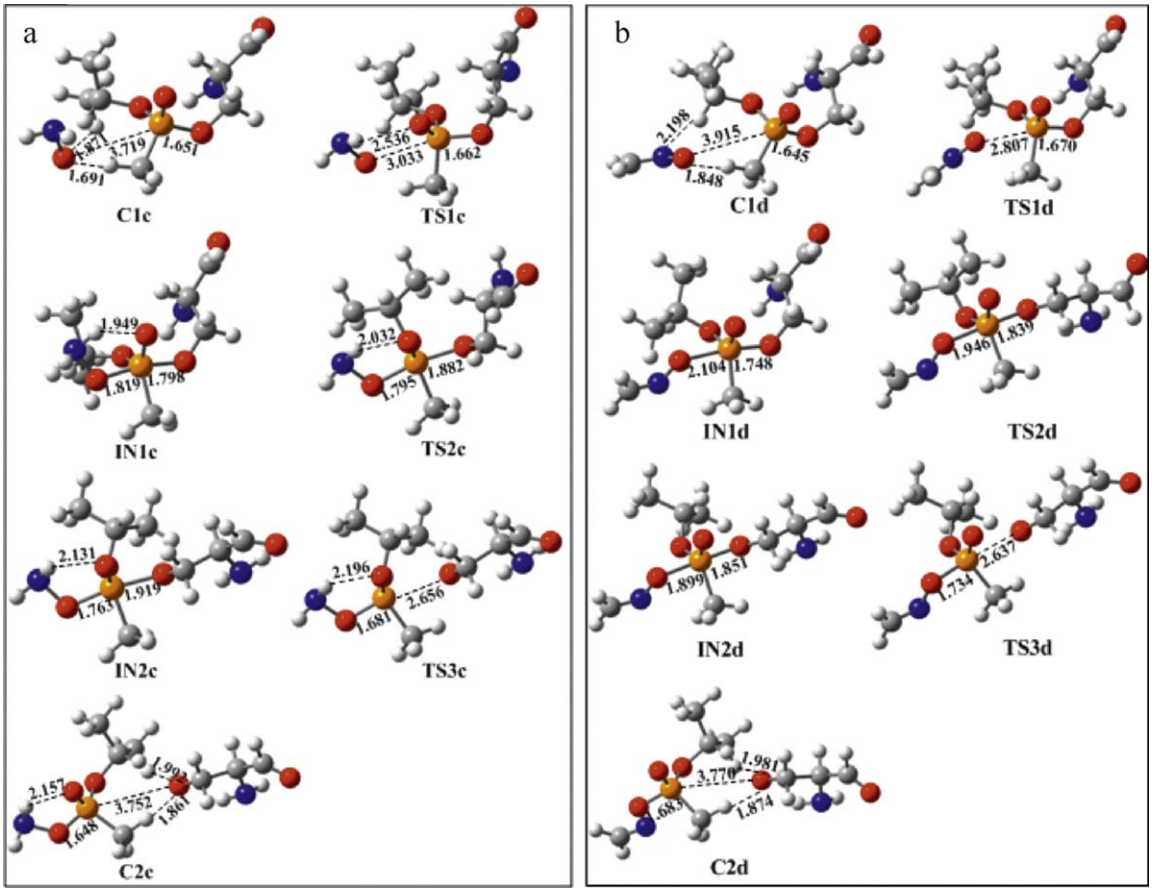

Fig. 6. B3LYP/6-311G(d,p) optimized geometries and selected bond distances (Å) for the reactivation process of sarin–serine adduct 3 with: (a) hydroxylamine anion and (b) formoximate anion in gas phase (grey = carbon, red = oxygen; blue = nitrogen; white = hydrogen; orange = phosphorus).

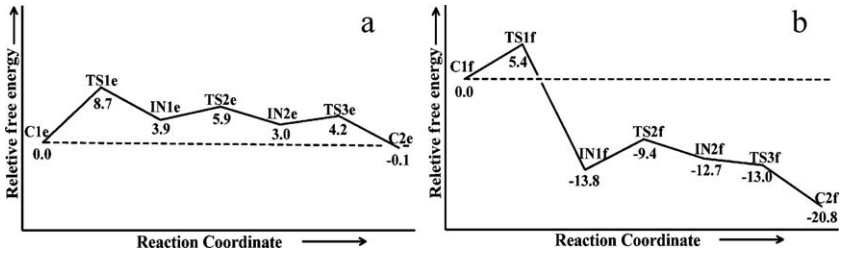

Fig. 7. B3LYP/6-311G(d,p) calculated free energy (kcal/mol) profile diagrams for the reactivation process of sarin–serine adduct 4 with: (a) formoximate anion and (b) hydroxylamine anion in gas phase.

in the gas phase results (Fig. 7a and Fig. S1e of the supplementary data).

Further, we have extended our study to examine the role of the carbonyl group adjacent to Glu202 with hydroxylamine anion and adduct 4. The calculated PES shows that the reaction process is similar in nature as observed in the absence of this carbonyl group (Figs. 5a and 7b). The optimized geometries in this case are provided in Fig. 8b. The activation barrier calculated for the attack (TS1f) of hydroxylamine anion to the adduct 4 is 3.3 kcal/mol lower than that of the formoximate anion. The calculated rate determined for the reactivation process of adduct 4 with NH_2O^- was found to be 261 times faster than the formoximate anion. Further, the inverse reactivation barrier with NH_2O^- is higher by 17.4 kcal/mol compared to the corresponding barrier with formoximate anion. The solvent phase calculations showed that the TS3f is 2.3 kcal/mol higher in energy than the intermediate IN2f; however, the TS3f was predicted to be lower in energy by 0.3 kcal/mol than the preceding intermediate in the gas phase calculations (Fig. 7b and Fig. S1f of the supplementary data) [20,21].

In the crystal structure of the sarin inhibited AChE, phosphonyl oxygen of sarin moiety forms intermolecular hydrogen bonds with the backbone –NH groups of Gly121, Gly122 and Ala204 (Fig. 9) [47]. The presence of these nitrogen residues in the active site of AChE is known as oxyanion hole. Therefore, to examine the effect of these intermolecular hydrogen bondings to the reactivation process of sarin inhibited AChE with formoximate and hydroxylamine anions, additional calculations have been performed with the adduct 4. We have modeled –NH groups of Gly121 and Gly122 as hydrogen bond donors, while performing the calculations as shown in Figs. S3 and S5 of the supplementary data. The –NH group of Ala204 is not included in the study, because it forms a very weak hydrogen bond with the P═O oxygen [47]. The calculated potential energy surfaces are shown in Figs. S2 and S4 of the supplementary data.

The influence of intermolecular hydrogen bonding on the PES of hydroxylamine anion is minimal as the relative energies of the stationary points are almost similar to the situation where such hydrogen bonding interactions are absent (Fig. S2 of the supplementary data and Fig. 7b). The computed PES for formoximate anion with 4, however, showed that the reaction process is slightly endothermic in nature in presence of hydrogen bonding from –NH groups of Gly121 and Gly122 (Fig. S4 of the supplementary data).

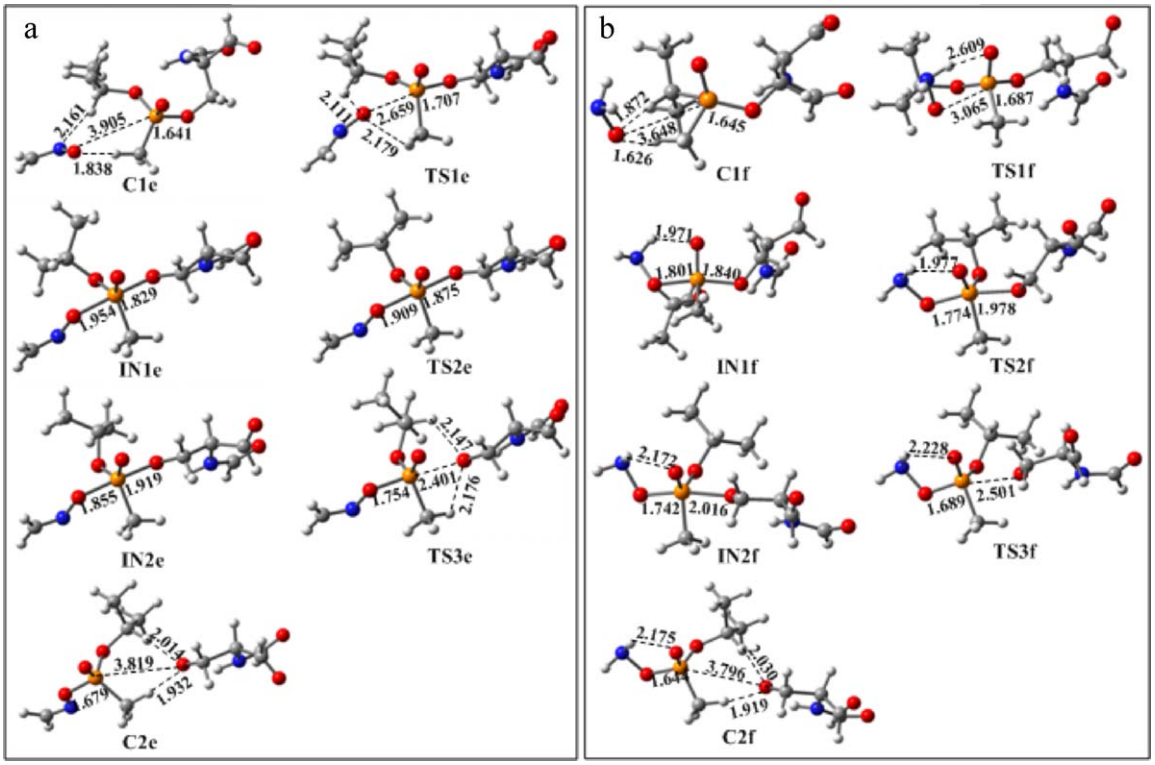

Fig. 8. B3LYP/6-311G(d,p) optimized geometries and selected bond distances (Å) for the reactivation process of sarin–serine adduct 4 with: (a) formoximate anion and (b) hydroxylamine anion in gas phase (grey = carbon, red = oxygen; blue = nitrogen; white = hydrogen; orange = phosphorus). (For interpretation of the references to color in this figure legend, the reader is referred to the web version of the article.)

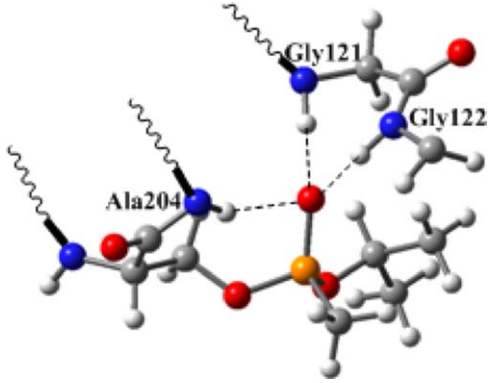

Fig. 9. Crystal structure of sarin inhibited AChE. Dashed lines represent the formation of hydrogen bonds between phosphonyl oxygen of sarin and –NH groups of Gly121, Gly122 and Ala204. Wavy bonds represents remaining part of the enzyme (grey = carbon, red = oxygen; blue = nitrogen; white = hydrogen; orange = phosphorus). (For interpretation of the references to color in this figure legend, the reader is referred to the web version of the article.)

The relative trend towards the efficacy of hydroxylamine anion for the reactivation process is better than the formoximate anion in the presence of the intermolecular hydrogen bonding of phosphonyl oxygen of sarin moiety with Gly121 and Gly122. The predicted rate constant indicates that the NH_2O^- should be faster by 223 times than the formoximate anion for the reactivations of sarin–serine adduct 4 in the presence of such hydrogen bonding. The imidazole moiety of histidine in the catalytic triad of AChE participates in the reactivation and the aging processes [48–50]. The roles of protonated imidazole for reactivation of sarin–serine adduct 4 with NH_2O^- and formoximate anions were also examined. The calculations performed with the protonated imidazole ring showed that the process is slightly more exergonic with NH_2O^-, however, more endergonic in the case of formoximate anion (Fig. S6 of the supplementary data).

4. Conclusions

In the present work, density functional calculations have been performed employing B3LYP/6-311G(d,p) for the reactivation process of sarin-inhibited AChE with hydroxylamine anion and formoximate anion. The computed free energy of activation (2.3 kcal/mol) for the reactivation of sarin-inhibited AChE (modeled sarin–serine adduct 2) is lower with hydroxylamine anion compared to other nucleophiles reported. The calculated results further suggest that NH_2O^- should be a better reactivating agent for sarin-inhibited AChE compared to the formoximate anion even with other sarin–serine adducts 3 and 4. The computed results shed light on the importance of the adjacent carbonyl group of Glu202 for the reactivation process of sarin–serine adduct with formoximate anion. The participation of carbonyl group of Glu202 in the reactivation of adduct 4 reduces the activation barrier by 3.1 kcal/mol compared to that of adduct 3 where such carbonyl group is not present. The performance of hydroxylamine anion to reactivate the sarin-inhibited AChE with sarin–serine adduct 4 was found to be superior to formoximate anion with intermolecular hydrogen bonding interactions of Gly121 and Gly122 as well. The isopropoxy moiety in the sarin–serine adduct 3 increased the activation barriers with the hydroxylamine anion and formoximate anion compared to the methoxy moiety present in adduct 2, however, the efficacy of NH_2O^- remain the same in both cases [22]. Higher free energy of activation for the reverse reactivation reaction between NH_2O^- and sarin–serine adduct, further suggests that this α-nucleophile can be a very good antidote agent for the reactivation process.

Acknowledgments

Authors thank DAE-BRNS, Mumbai, and DST, New Delhi, India for financial support of this work. One of the authors MASK is thankful to DAE-BRNS and RL is thankful to UGC, New Delhi, India for awarding fellowship.

Appendix A. Supplementary data

Supplementary data associated with this article can be found, in the online version, at doi:10.1016/j.jmgm.2011.04.009.

References

[1] C.A. Buntun, Chemical warfare in Macmillan encyclopedia of chemistry, in: J.J. Lagowsky (Ed.), Macmillan Reference USA, vol. 1, Simon and Schuster Macmillan, New York, 1997, pp. 343–346.
[2] J.J. DeFrank, Organophosphorus cholinesterase inhibitors: detoxification by microbial enzymes, in: J.W. Kelly, T.O. Baldwin (Eds.), Applications of Enzyme Biotechnology, Plenum Press, New York, 1991, pp. 165–180.
[3] E. Heilbronn-Wikstrom, Phosphorylated cholinesterase: their formation reactions and hydrolysis, Sven. Kem. Tidskr. 77 (1965) 598–631.
[4] H.C. Kolb, K.B. Sharpless, The growing impact of click chemistry on drug discovery, Drug Discov. Today 8 (2003) 1128–1137.
[5] D.M. Quinn, Acetylcholinesterase: enzyme structure, reaction dynamics and virtual transition states, Chem. Rev. 87 (1987) 955–979.
[6] A. Shafferman, C. Kronman, Y. Flashner, M. Leitner, H. Grosfeld, A. Ordentlich, Y. Gozes, S. Cohen, N. Ariel, D. Barak, M. Harel, I. Silman, J.L. Sussman, B. Velan, Mutagenesis of human acetylcholinesterase identification of residues involved in catalytic activity and in polypeptide folding, J. Biol. Chem. 267 (1992) 17640–17648.
[7] J. Wang, S. Roszak, J. Gu, J. Leszczynski, Comprehensive global energy minimum modeling of the sarin–serine adduct, J. Phys. Chem. B 109 (2005) 1006–1014.
[8] J. Wang, J. Gu, J. Leszczynski, Phosphonylation mechanisms of sarin and acetylcholinesterase: a model DFT study, J. Phys. Chem. B 110 (2006) 7567–7573.
[9] P. Taylor, S. Lappi, Interaction of fluorescence probes with acetylcholinesterase site and specificity of propidium binding, Biochemistry 14 (1975) 1989–1997.
[10] M. Eddleston, L. Szinicz, P. Eyer, N. Buckley, Oximes in acute organophosphorus pesticide poisoning: a systematic review of clinical trials, QJM – Assoc. Int. J. Med. 95 (2002) 275–283.
[11] F. Berends, C.H. Posthumus, I.V.D. Sluys, F.A. Deierkauf, Biochim. Biophys. Acta 34 (1959) 576–579.
[12] L. Wong, Z. Radić, R.J.M. Brüggemann, N. Hosea, H.A. Berman, P. Taylor, Mechanism of oxime reactivation of acetylcholinesterase analyzed by chirality, and mutagenesis, Biochemistry 39 (2000) 5750–5757.
[13] V.M. Bermudez, Computational study of the adsorption of trichlorophosphate, dimethyl methylphosphonate, and sarin on amorphous SiO_2, J. Phys. Chem. C 111 (2007) 9314–9323.
[14] I. Bandyopadhyay, M.J. Kim, Y.S. Lee, D.G. Churchill, Favorable pendant-amino metal chelation in VX nerve agent model systems, J. Phys. Chem. A 110 (2006) 3655–3661.
[15] J. Šečkutė, J.L. Menke, R.J. Emnett, E.V. Patterson, C.J. Cramer, Ab initio molecular orbital, and density functional studies on the solvolysis of sarin and *O,S*-dimethyl methylphosphonothiolate, a VX-like compound, J. Org. Chem. 70 (2005) 8649–8660.
[16] F. Zheng, C.G. Zhan, R.L. Ornstein, Theoretical studies of reaction pathways and energy barriers for alkaline hydrolysis of phosphotriesterase substrates paraoxon and related toxic phosphofluoridate nerve agents, J. Chem. Soc. Perkin Trans. 2 (2001) 2355–2363.
[17] E.V. Patterson, C.J. Cramer, Molecular orbital calculations on the P–S bond cleavage step in the hydroperoxidolysis of nerve agent VX, J. Phys. Org. Chem. 11 (1998) 232–240.
[18] K.A. Daniel, L.A. Kopff, E.V. Patterson, Computational studies on the solvolysis of the chemical warfare agent VX, J. Phys. Org. Chem. 21 (2008) 321–328.
[19] J.L. Menke, E.V. Patterson, Quantum mechanical calculations on the reaction of ethoxide anion with *O,S*-dimethyl methylphosphonothiolate, J. Mol. Struct. THEOCHEM 811 (2007) 281–291.
[20] M.A.S. Khan, M.K. Kesharwani, T. Bandyopadhyay, B. Ganguly, Solvolysis of chemical warfare agent VX is more efficient with hydroxylamine anion: a computational study, J. Mol. Graphics Model. 28 (2009) 177–182.
[21] M.A.S. Khan, M.K. Kesharwani, T. Bandyopadhyay, B. Ganguly, Remarkable effect of hydroxylamine anion towards the solvolysis of sarin: a DFT study, J. Mol. Struct. THEOCHEM 944 (2010) 132–136.
[22] J. Wang, J. Gu, J. Leszczynski, M. Feliks, W.A. Sokalski, Oxime-induced reactivation of sarin-inhibited AChE: a theoretical mechanisms study, J. Phys. Chem. B 111 (2007) 2404–2408.
[23] J. Wang, J. Gu, J. Leszczynski, Theoretical modeling study for the phosphonylation mechanisms of the catalytic triad of acetylcholinesterase by sarin, J. Phys. Chem. B 110 (2006) 7567–7573.
[24] R.T. Delfino, J.D. Figueroa-Villar, Nucleophilic reactivation of sarin-inhibited acetylcholinesterase: a molecular modeling study, J. Phys. Chem. B 113 (2009) 8402–8411.

[25] F. Mohamdi, N.G.J. Richards, W.C. Guida, R. Liskamp, M. Lipton, C. Caufield, G. Chang, T. Hendrickson, W.C. Still, Macromodel – an integrated software system for modeling organic and bioorganic molecules using molecular mechanics, J. Comput. Chem. 11 (1990) 440–467.
[26] T.A. Halgren, Merck molecular force field. V. Extension of MMFF94 using experimental data, additional computational data, and empirical rules, J. Comput. Chem. 17 (1996) 616–641.
[27] T.A. Halgren, Merck molecular force field. III. Molecular geometries and vibrational frequencies for MMFF94, J. Comput. Chem. 17 (1996) 553–586.
[28] T.A. Halgren, Merck molecular force field. II. MMFF94 van der Waals and electrostatic parameters for intermolecular interactions, J. Comput. Chem. 17 (1996) 520–552.
[29] T.A. Halgren, Merck molecular force field. I. Basis, form, scope, parameterization, and performance of MMFF94, J. Comput. Chem. 17 (1996) 490–519.
[30] T.A. Halgren, R.B. Nachbar, Merck molecular force field. IV. Conformational energies and geometries for MMFF94, J. Comput. Chem. 17 (1996) 587–615.
[31] E. Polak, G. Ribiere, Note surla convergence des methodes de directions conjuguees, Rev. Fr. Inf. Rech. Oper. 16-R1 (1969) 35–43.
[32] G. Chang, W.C. Guida, W.C. Still, An internal-coordinate Monte Carlo method for searching conformational space, J. Am. Chem. Soc. 111 (1989) 4379–4386.
[33] M. Saunders, K.N. Houk, Y.D. Wu, W.C. Still, M. Lipton, G. Chang, W.C. Guida, Conformations of cycloheptadecane. A comparison of methods for conformational searching, J. Am. Chem. Soc. 112 (1990) 1419–1427.
[34] P.S. Shenkin, D.Q. McDonald, Cluster analysis of molecular conformations, J. Comput. Chem. 15 (1994) 899–916.
[35] S.D. Hillson, E. Smith, M. Zeldin, C.A. Parish, Cages, baskets, ladders, and tubes: conformational studies of polyhedral oligomeric silsesquioxanes, J. Phys. Chem. A 109 (2005) 8371–8378.
[36] A.D. Becke, Density-functional thermo chemistry III. The role of exact exchange, J. Chem. Phys. 98 (1993) 5648–5652.
[37] C. Lee, W. Yang, R.G. Parr, Development of the Colle–Salvetti correlation-energy formula into a functional of the electron density, Phys. Rev. B 37 (1988) 785–789.
[38] J.M. Beck, C.M. Hadad, Hydrolysis of nerve agents by model nucleophiles: a computational study, Chem. Biol. Interact. 175 (2008) 200–203.
[39] J. Tomasi, M. Persico, Molecular interactions in solution: an overview of methods based on continuous distributions of the solvent, Chem. Rev. 94 (1994) 2027–2094.
[40] M. Cossi, V. Barone, R. Cammi, J. Tomasi, Ab initio study of solvated molecules: a new implementation of the polarizable continuum model, Chem. Phys. Lett. 255 (1996) 327–335.
[41] V. Barone, M. Cossi, J. Tomasi, A new definition of cavities for the computation of solvation free energies by the polarizable continuum model, J. Chem. Phys. 107 (1997) 3210–3221.
[42] V. Barone, M. Cossi, J. Tomasi, Geometry optimization of molecular structures in solution by the polarizable continuum model, J. Comput. Chem. 19 (1998) 404–417.
[43] M. Cossi, V. Barone, Analytical second derivatives of the free energy in solution by polarizable continuum models, J. Chem. Phys. 109 (1998) 6246–6254.
[44] C. González, H.B. Schlegel, Reaction path following in mass-weighted internal coordinates, J. Phys. Chem. 94 (1990) 5523–5527.
[45] C. González, H.B. Schlegel, Improved algorithms for reaction path following: higher-order implicit algorithms, J. Chem. Phys. 95 (1991) 5853–5860.
[46] M.J. Frisch, G.W. Trucks, H.B. Schlegel, G.E. Scuseria, M.A. Robb, J.R. Cheeseman, J.A. Montgomery Jr., T. Vreven, K.N. Kudin, J.C. Burant, J.M. Millam, S.S. Iyengar, J. Tomasi, V. Barone, B. Mennucci, M. Cossi, G. Scalmani, N. Rega, G.A. Petersson, H. Nakatsuji, M. Hada, M. Ehara, K. Toyota, R. Fukuda, J. Hasegawa, M. Ishida, T. Nakajima, Y. Honda, O. Kitao, H. Nakai, M. Klene, X. Li, J.E. Knox, H.P. Hratchian, J.B. Cross, V. Bakken, C. Adamo, J. Jaramillo, R. Gomperts, R.E. Stratmann, O. Yazyev, A.J. Austin, R. Cammi, C. Pomelli, J.W. Ochterski, P.Y. Ayala, K. Morokuma, G.A. Voth, P. Salvador, J.J. Dannenberg, V.G. Zakrzewski, S. Dapprich, A.D. Daniels, M.C. Strain, O. Farkas, D.K. Malick, A.D. Rabuck, K. Raghavachari, J.B. Foresman, J.V. Ortiz, Q. Cui, A.G. Baboul, S. Clifford, J. Cioslowski, B.B. Stefanov, G. Liu, A. Liashenko, P. Piskorz, I. Komaromi, R.L. Martin, D.J. Fox, T. Keith, M.A. Al-Laham, C.Y. Peng, A. Nanayakkara, M. Challacombe, P.M.W. Gill, B. Johnson, W. Chen, M.W. Wong, C. Gonzalez, J.A. Pople, Gaussian 03, Revision E. 01, Gaussian, Inc., Wallingford, CT, 2004.
[47] A. Hörnberg, A.-K. Tunemalm, F. Ekström, Crystal structures of acetylcholinesterase in complex with organophosphorus compounds suggest that the acyl pocket modulates the aging reaction by precluding the formation of the trigonal bipyramidal transition state, Biochemistry 46 (2007) 4815–4825.
[48] E. Carletti, J.-P. Colletier, F. Dupeux, M. Trovaslet, P. Masson, F. Nachon, Structural evidence that human acetylcholinesterase inhibited by tabun ages through O-dealkylation, J. Med. Chem. 53 (2010) 4002–4008.
[49] F. Nachon, E. Carletti, F. Worek, P. Masson, Aging mechanism of butyrylcholinesterase inhibited by an N-methyl analogue of tabun: implications of the trigonal–bipyramidal transition state rearrangement for the phosphylation or reactivation of cholinesterases, Chem. Biol. Interact. 187 (2010) 44–48.
[50] E. Carletti, H. Li, B. Li, F. Ekström, Y. Nicolet, M. Loiodice, E. Gillon, M.T. Froment, O. Lockridge, L.M. Schopfer, P. Masson, F. Nachon, Aging of cholinesterases phosphylated by tabun proceeds through O-dealkylation, J. Am. Chem. Soc. 130 (2008) 16011–16020.